Hydrogen Evolution

Deutsche Ausgabe: DOI: 10.1002/ange.201603021
Internationale Ausgabe: DOI: 10.1002/anie.201603021

Facet-Dependent and Light-Assisted Efficient Hydrogen Evolution from Ammonia Borane Using Gold–Palladium Core–Shell Nanocatalysts

*Sourav Rej, Chi-Fu Hsia, Tzu-Yu Chen, Fan-Cheng Lin, Jer-Shing Huang, and Michael H. Huang**

Abstract: *Au–Pd core–shell nanocrystals with tetrahexahedral (THH), cubic, and octahedral shapes and comparable sizes were synthesized. Similar-sized Au and Pd cubes and octahedra were also prepared. These nanocrystals were used for the hydrogen-evolution reaction (HER) from ammonia borane. Light irradiation can enhance the reaction rate for all the catalysts. In particular, Au–Pd THH exposing {730} facets showed the highest turnover frequency for hydrogen evolution under light with 3-fold rate enhancement benefiting from lattice strain, modified surface electronic state, and a broader range of light absorption. Finite-difference time-domain (FDTD) simulations show a stronger electric field enhancement on Au–Pd core–shell THH than those on other Pd-containing nanocrystals. Light-assisted nitro reduction by ammonia borane on Au–Pd THH was also demonstrated. Au–Pd tetrahexahedra supported on activated carbon can act as a superior recyclable plasmonic photocatalyst for hydrogen evolution.*

Plasmonic metal nanocrystals such as Au, Ag, and Pd have been synthesized in aqueous solutions with well-defined shapes, such as cubic and octahedral structures.[1–7] Their clean surfaces have enabled the evaluation of facet effects on organocatalysis with product selectivity.[8–10] Similarly, bimetallic Au–Pd and Au–Ag core–shell nanocrystals with tunable shapes and sizes can also be prepared in aqueous solutions and be used for facet-dependent catalytic examinations.[11–16] It has been shown that Pd nanocrystals are not only useful in various organic reactions but they can also be applied for hydrogen gas production through dehydrogenation of ammonia borane (NH_3BH_3).[17–22] Ammonia borane (AB) is a promising hydrogen-storage material because of its high hydrogen storage capacity (19.6 wt%) among all practical hydrogen-storage materials.[23,24] It is highly soluble in water and inert toward hydrolysis, but produces hydrogen gas only in the presence of a suitable catalyst.[17–20,25–28] Development of simple and highly efficient catalysts for the dehydrogenation of AB is desirable. Previous notable examples used sub-10 nm spherical Pd and CoPd alloy nanoparticles to catalyze this reaction.[17–20] Facet effects on catalytic efficiency have not been examined for this reaction. It should be interesting to use cubic and octahedral Pd nanocrystals for the dehydrogenation of AB.

In addition to employing pure Pd nanocrystals as the catalyst, use of polyhedral Au–Pd core–shell heterostructures for hydrogen generation can be advantageous because Pd surface property can be modified slightly by the Au cores, and the particles can absorb a wider range of visible light. Such nanostructures can be used in plasmonic photocatalysis to improve catalytic efficiency. For example, bimetallic AuPd nanowheels can serve as a highly efficient catalyst in the oxidation of benzyl alcohol and Suzuki coupling reaction under light irradiation.[29] Pd-tipped Au nanorods have exhibited plasmon-enhanced formic acid dehydrogenation and Suzuki coupling reactions compared with conventional thermal catalysis.[30,31] Thus, it is interesting to compare catalytic efficiency of polyhedral Pd and Au–Pd core–shell nanocrystals exposing different surfaces for dehydrogenation of AB without and under light irradiation.

In this study, we have prepared Au–Pd core–shell THH, cubes and octahedra and compared their catalytic activities with those of pure Pd and Au cubic and octahedral nanocrystals for the hydrogen evolution reaction from AB. The nanocrystals were synthesized in aqueous solutions using cetyltrimethylammonium chloride (CTAC) or cetyltrimethylammonium bromide (CTAB) as surfactant and ascorbic acid as reductant to keep the surface chemistry almost same. To make Au–Pd core–shell nanocrystals, cubic and octahedral Au cores were prepared following a seed-mediated growth method.[32,33] A tiny amount of NaBr was added for the growth of Au nanocubes, whereas KI was introduced to obtain Au octahedra. Figure S1 in the Supporting Information shows SEM images and size distribution histograms of the synthesized Au nanocubes and octahedra with an average size of 32 and 33 nm, respectively. A sharp localized surface plasmon resonance (LSPR) absorption band at 527 and 531 nm was observed for the Au nanocubes and octahedra, respectively (see Figure S1). Au-Pd core–shell THH nanocrystals (ca. 82 nm in opposite corner distance) were synthesized from an aqueous mixture of CTAC, cubic Au cores, H_2PdCl_4, and ascorbic acid. The high-index {730} facets in THH particles are formed to release the lattice strain, which arises from the lattice mismatch between Au and Pd (ca. 4.61%) and simultaneous oxidative etching by both chloride ions and dissolved oxygen.[11] We have developed a new

[*] Dr. S. Rej, C.-F. Hsia, T.-Y. Chen, F.-C. Lin, Prof. J.-S. Huang, Prof. M. H. Huang
Department of Chemistry
National Tsing Hua University
Hsinchu 30013 (Taiwan)
E-mail: hyhuang@mx.nthu.edu.tw

Supporting information and the ORCID identification number(s) for the author(s) of this article can be found under http://dx.doi.org/10.1002/anie.201603021.

synthetic condition to grow highly uniform Au–Pd core–shell cubes (ca. 59 nm) using 32 nm cubic Au cores, CTAB surfactant, H_2PdCl_4, and ascorbic acid at 50 °C for 1 h. Au-Pd core–shell octahedra (~53 nm) were prepared using 33 nm octahedral Au cores.[13] Apart from core–shell particles, 60 nm Pd cubes and 61 nm octahedra have also been synthesized.[3] Similarly, 54 and 59 nm Au cubes and octahedra were also prepared.[32,33] Figure S2 provides size distribution histograms for all these particles.

Figure 1 presents SEM images of the synthesized nanocrystals, showing that all samples contain highly uniform

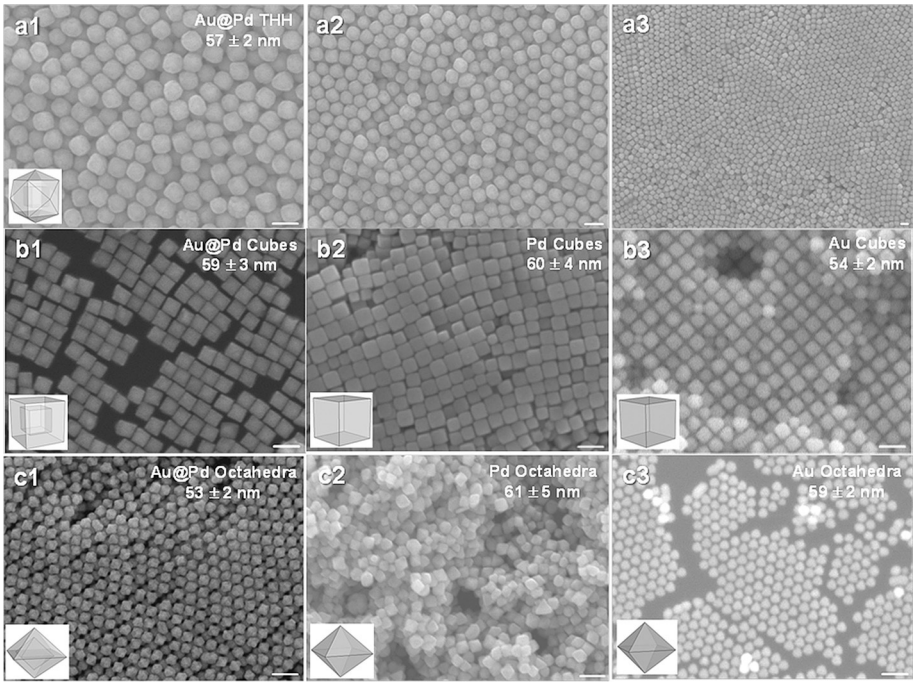

Figure 1. a1), a2), a3) SEM images of THH Au–Pd core–shell nanocrystals at different magnifications. b1), b2), b3) SEM images of b1) Au–Pd core–shell nanocubes, b2) Pd nanocubes, and b3) Au nanocubes. c1), c2), c3) SEM images of c1) Au–Pd core–shell octahedra, c2) Pd octahedra, and c3) Au octahedra. All scale bars are 100 nm. Particle models are shown. Average particle sizes and their standard deviations are provided.

nanocrystals. Owing to the high shape and size homogeneity, the particles easily self-assemble into ordered packing arrangements. TEM images of single Au-Pd core–shell nanocube, octahedron, and tetrahexahedron are shown in Figure S3. EDS line scans confirm the composition of the core and shell as Au and Pd, respectively in the three nanocrystals. By measuring the facet angles from a TEM image of one THH Au–Pd core–shell nanocrystal, it is concluded that the particle is bound by the {730} surfaces as shown in Figure S4.[11,34]

Figure S5 shows XRD patterns of Au–Pd core–shell THH, cubes, and octahedra with those of pure Pd cubes and octahedra. Pd octahedra show an exceptionally strong (111) reflection peak, while the (200) peak is dominant for Pd cubes due to their preferred orientation of deposition on substrates. Similar orientation-enhanced XRD patterns can also be seen in Au-Pd core–shell nanocrystals. Peak intensities for Au are much stronger than those of Pd in Au–Pd octahedra because of the thin Pd shells. The corresponding Au and Pd peaks (for example, the (200) peaks) show the same orientation-induced intensity effect, indicating they have an exact lattice orientation relationship. While the peak positions for Au match with its standard pattern in the case of Au–Pd THH particles, the Pd (111) and (200) peaks are shifted to lower 2θ angles with respect to its standard peak positions by 0.47° and 0.69° for the Pd (111) and Pd (200) peaks, respectively. This lattice expansion comes from the strain effect between Au and Pd. Such left-shift of the Pd (111) peak in Au–Pd core–shell octahedra has been observed with a shell thickness of less than 1 nm.[35] Here we show that lattice expansion can still be observed in Au–Pd THH nanocrystals with very thick Pd shells. Interestingly, for Au–Pd core–shell nanocubes and octahedra, it is the Au (200) peaks showing slight right-shift by 0.20–0.25° 2θ. Similar right-shift for the Au peak was also recorded in various Au–Pd core–shell nanocrystals reported previously but not recognized at that time.[12]

For accurate facet-dependent catalytic activity comparison, total surface area of the particles was kept constant for all the samples. To have a fixed total surface area of 450 cm^2, different volumes of the nanocrystal solutions were used for the catalytic experiments (see the Supporting Information for the calculations). Figure 2a shows a plot of the volume of generated hydrogen gas versus time taken by various nanocatalysts from 0.3 mmol of AB both in dark and in the presence of light from a Xe lamp (power density 100 $mW\,cm^{-2}$). When 0.3 mmol of AB is completely hydrolyzed, it produces 0.9 mmol of H_2 (ca. 20 mL) indicating completion of the reaction as shown in Equation (1).

$$NH_3BH_3 + 2\,H_2O \rightarrow NH_4^+ + BO_2^- + 3\,H_2\uparrow \quad (1)$$

In the presence of different nanocatalysts, hydrogen production rates were found as follows: Au octahedra < Au cubes < Pd octahedra < Au–Pd octahedra < Pd cubes < Au–Pd cubes < Au-Pd tetrahexahedra. A-u-Pd THH nanocatalyst showed the highest catalytic activity among the different nanocatalysts. When the same experiment was carried out under light illumination from a Xe lamp, the catalytic activity order remains the same but each of them showed a different degree of enhanced photocatalytic activity. Again Au–Pd THH particles showed the largest photocatalytic rate enhancement compared to the others. Au octahedra and cubes showed the lowest catalytic efficiency for this reaction. Pd

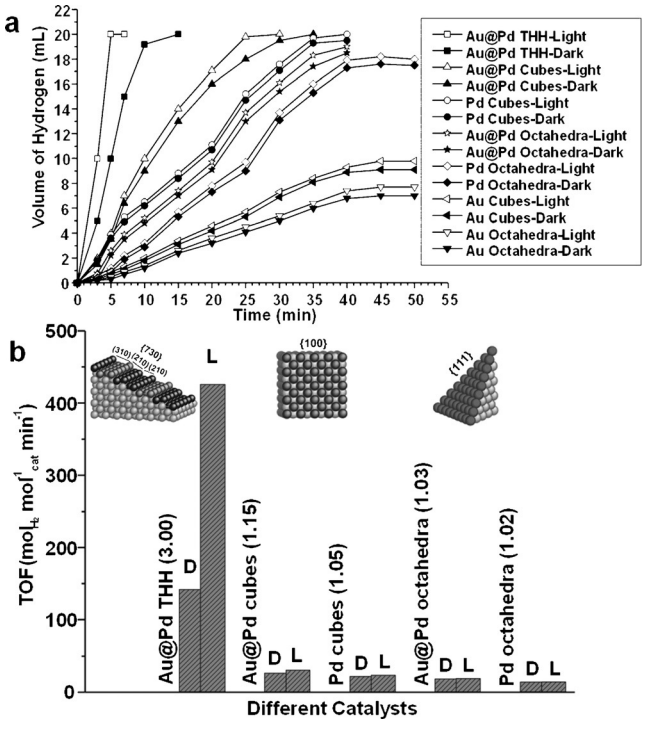

Figure 2. a) Plot for volume of hydrogen generated from ammonia borane hydrolysis versus time taken by different nanocrystals with and without light irradiation. Reaction conditions: normalized catalyst surface area = 450 cm^2, amount of ammonia borane used = 0.3 mmol, temperature = 25 °C. b) TOFs for the different catalysts in the dark (D) and in the presence of light (L). The value shown in the parenthesis is the TOF enhancement factor from dark to light.

octahedra showed a big jump in the hydrogen production rate compared to Au cubes, showing Pd's superior catalytic activity compared to Au toward dehydrogenation of AB. Au–Pd octahedra and Pd cubes took 40 min to generate 18.5 and 19.5 mL of H_2 respectively in the dark, whereas Au–Pd cubes needed 35 min to complete the reaction producing 20 mL of H_2 gas, suggesting that incorporation of Au cores can accelerate the reaction. Remarkably, Au–Pd THH nanocrystals finish the reaction in only 15 min in the dark. In the presence of light the reaction can be completed in just 5 min. Thus Au–Pd THH nanocrystals show around 3 times rate enhancement in the presence of light, which is unprecedented for the dehydrogenation of AB. Turnover frequencies (TOF), defined here as mol of H_2 produced per mol of surface Pd atoms per min, have been calculated for all the nanocrystals (see the Supporting Information). TOF value comparison for different catalysts in the dark and light are given in Figure 2b. Noticeably, the TOF values for Au–Pd THH nanocrystals in the dark and light are 142 and 426 $mol_{H2}\,mol_{cat}^{-1}\,min^{-1}$ respectively, which are highest among all the catalysts. The TOF values for Au–Pd and Pd nanocubes are 26 and 22 $mol_{H2}\,mol_{cat}^{-1}\,min^{-1}$, respectively, in dark. Figure S6 gives photographs of a solution of Au-Pd core–shell THH before catalysis and during the hydrogen evolution reaction. Gas bubbles can be seen over the entire cuvette. There is also a noticeable darkening of the solution color due to the incorporation of hydrogen atoms into the palladium lattice shifting the Au LSPR band position.[36] SEM image of the Au-Pd THH particles after the catalysis is available in Figure S7, showing preservation of particle shape.

To explain the observed catalytic activity, atomic arrangements of the exposed surface facets as seen in Figure 2b are compared. THH nanocrystals consist of high-index {730} facets show significantly higher catalytic activities compared to other low-index facets present in cubes and octahedra. The reason is that the {730} facets have significantly high fraction of surface atoms with a coordination number of 6, whereas the {100} and {111} surfaces have atomic coordination numbers of 8 and 9, respectively. A higher coordination number means a lower binding affinity of AB onto the surface atoms, so catalytic activity decreases from THH particles to cubes to octahedra.

The higher catalytic activity of the core–shell nanocrystals compared to their pure counterparts with similar size and shape in the dark condition can be explained considering the ligand effect or heterometallic bonding interaction. In Au–Pd particles, electrons will flow from Au with a smaller work function ($\Phi_{Au} \approx 5.3$ eV) to Pd, which has a slightly larger work function ($\Phi_{Pd} \approx 5.6$ eV), until the equilibrium is reached between core and shell and their chemical potentials become equal everywhere in the core–shell nanocrystal.[37] To investigate this ligand effect, XPS spectra were taken on Pd cubes and Au–Pd core–shell cubes and THH. Figure S8a,b shows the full XPS spectra of the Au–Pd THH and cubic nanocrystals taken before catalysis, confirming that the nanocrystal surfaces are fully cleaned and there is no detectable amount of CTAC, CTAB or other surface-adsorbed impurities, which is very important for facet-dependent catalytic activity comparison.[3] Figure S8c indicates that the binding energies of Pd 3d peaks in Au–Pd core–shell cubes are shifted to lower values compared to those of Pd cubes. The Pd $3d_{5/2}$ and $3d_{3/2}$ binding energies for Pd cubes are at 334.89 and 340.22 eV respectively, whereas those peaks for Au–Pd cubes are at 334.76 and 340.04 eV. This slight decrease in the binding energy proves electron redistribution between the Au core and Pd shell. The Pd $3d_{5/2}$ and $3d_{3/2}$ binding energies in Au-Pd THH particles are 334.82 and 340.13 eV, respectively. The modified surface electronic structure in core–shell nanocrystals alters the interaction between AB and surface Pd atoms, showing their enhanced catalytic properties.

The enhanced hydrogen production rate in the presence of light can be explained by considering UV/Vis absorption spectra of the different Pd and Au–Pd nanocrystals (Figure S9). Au–Pd core–shell nanocrystals always show a broader absorption profile into the visible light region compared to Pd cubes and octahedra because of the Au core. In particular, Au–Pd core–shell THH nanocrystals show a LSPR band maximum at 450 nm with the broadest absorption tail covering the entire visible light range into the near-infrared region. Thus they can harvest more visible light to carry out the plasmonic photocatalysis most efficiently. Since full-spectrum Xe lamp irradiation has been used without using any optical filter in the photocatalytic reaction, contribution from the photothermal effect needs to be considered. We have measured the temperature increase of the aqueous solution

containing THH nanocrystals in the presence of full-spectrum irradiation. A temperature increase of only 2 °C was observed over 15 min of irradiation. Figure S10 shows there is no significant increase in the hydrogen production rate at 27 °C compared to that at 25 °C, thus photothermal effect has no significant contribution to enhance the dehydrogenation reaction.

A schematic diagram for the dehydrogenation mechanism of AB in the presence of metal nanocatalyst is presented in Figure S11. The enhanced hydrogen production rate in the presence of light by Au–Pd core–shell THH nanocatalyst can be explained by considering the localized surface plasmon resonance effect. Recently, Yamashita et al. have shown that surface charge separation generated by the collective oscillations of free electrons on Ag nanoparticles are responsible for the activation of AB, resulting in enhanced hydrogen production in the presence of light.[25] Similarly, Majima et al. showed that Pd-tipped Au nanorods produces a large extent of surface charge heterogeneity on the co-exposed Pd and Au surfaces in the presence of light, and hence an improved hydrogen production rate from formic acid in the presence of light.[30] To determine the region of electric field amplification upon SPR excitation as a function of incident polarization direction and the role of surface charge heterogeneity on the dehydrogenation of AB, 3D-FDTD simulations were performed and shown in Figure S12. It clearly indicates that the near-field resonances are distributed along the edges or corners of nanocrystals with cubic, octahedral, and THH shapes. According to the Mie theory, it is easy to imagine that the density of surface hot electrons along the edges or corners is larger than a uniform area.[38] XPS spectra and XRD patterns have shown that core–shell nanocrystals have modified surface electronic properties. When these core–shell nanocrystals are exposed to light, much more efficient electron transfer takes place from the Au core to the Pd shell,[29–31] and the generated hot electrons get more concentrated along the edges and corners of the well-defined nanocrystals, making the uniform area more electron-deficient which produces enhanced surface charge heterogeneity. THH nanocrystals contain the highest number of edges and corners followed by cubes and octahedra, so it is expected that they will produce a higher degree of surface charge heterogeneity in the presence of light. The protonic hydrogens of NH_3 in AB prefer to attach to the corner and edge palladium atoms, which are more electron-rich in the presence of light. Similarly, the hydridic hydrogens of BH_3 part prefer the planar areas. Thus surface charge heterogeneity on the nanocrystal surface in the presence of light favors enhanced binding of AB which effectively reduces the activation barrier and weakens the B–N bond in AB. Furthermore, when these hot electrons revert back to their original state, they release their excess energy which can also be transferred to the surface-attached AB molecules, thus weakening the B–N bond. H_2O molecules subsequently attack on these weakened "B–N" bonds to generate BH_3 intermediates, which then undergo hydrolysis to release hydrogen gas. Thus activation of AB takes place more efficiently in the presence of light resulting in enhanced hydrogen production.

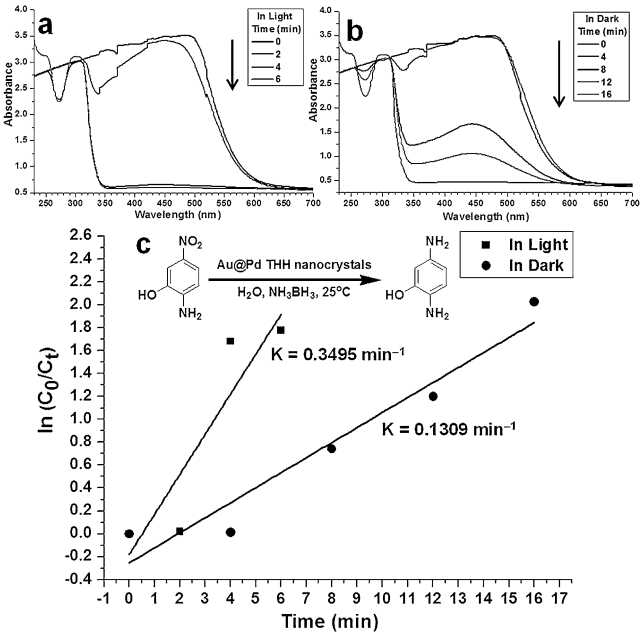

Figure 3. Time-dependent UV/Vis absorption spectra for the reduction of 2-amino-5-nitrophenol by ammonia borane in the presence of Au–Pd core–shell THH nanocrystals a) with light and b) without light at 25 °C. c) $\ln[C_0/C_t]$ versus time plot for the reaction with and without light irradiation.

Figure 3 shows the reduction of 2-amino-5-nitrophenol by AB in the presence of Au–Pd core–shell THH nanocrystals with and without light irradiation. Figure S13 confirms selective formation of 2,5-diaminophenol. At 25 °C, the reduction rate constants in light and dark are 0.3495 and 0.1309 min^{-1}, respectively (Figure 3c), indicating an enhancement of 2.67-fold due to the light energy. Figure S14 confirms that in the absence of Pd surface no nitro reduction takes place. In the presence of light, local hydride concentration on the nanocrystal surface are much higher compared to dark, which catalyze efficient electron transfer from the donor H^- to the acceptor 2-amino-5-nitrophenol, resulting in enhanced reduction rate. Au–Pd THH particles were also deposited on activated carbon to prepare recyclable catalyst. Figure S15 gives volume of hydrogen produced with respect to time in the presence of light for 3 cycles of the reactions. Consistently good hydrogen production has been demonstrated. TEM images of the Au-Pd THH/C catalyst before and after the reactions show their good reusability.

In conclusion, we have synthesized Au–Pd bimetallic core–shell nanocrystals with THH, cubic, and octahedral shapes and compared their plasmonic photocatalytic activity for dehydrogenation reaction of AB with comparable-sized Pd and Au cubes and octahedra. The Au–Pd THH particles displayed exceptionally high reactivity with the highest TOF value and three-fold rate enhancement in the presence of light, which has been well explained using XRD, XPS, UV/Vis spectra, and 3D-FDTD simulations. A plasmon-enhanced nitro reduction reaction was recorded. This study shows how thoughtful choice of facet and incorporation of a plasmonic core in a nanocrystal can modify the particle's surface

electronic structure and light harvesting properties to produce energy-efficient plasmonic photocatalysts.

Acknowledgements

We thank the Ministry of Science and Technology of Taiwan for the support of this research (Grants 104-2118-M-007-073 and 101-2113-M-007-018-MY3).

Keywords: facet-dependent properties · hydrogen evolution · nanocrystals · palladium · plasmonic photocatalysis

How to cite: *Angew. Chem. Int. Ed.* **2016**, *55*, 7222–7226
Angew. Chem. **2016**, *128*, 7338–7342

[1] M. R. Langille, M. L. Personick, J. Zhang, C. A. Mirkin, *J. Am. Chem. Soc.* **2012**, *134*, 14542.
[2] W. Niu, L. Zhang, G. Xu, *ACS Nano* **2010**, *4*, 1987.
[3] S.-Y. Liu, Y.-T. Shen, C.-Y. Chiu, S. Rej, P.-H. Lin, Y.-C. Tsao, M. H. Huang, *Langmuir* **2015**, *31*, 6538.
[4] J. Zhang, C. Feng, Y. Deng, L. Liu, Y. Wu, B. Shen, C. Zhong, W. Hu, *Chem. Mater.* **2014**, *26*, 1213.
[5] H.-X. Zhang, H. Wang, Y.-S. Re, W.-B. Cai, *Chem. Commun.* **2012**, *48*, 8362.
[6] Z.-W. Lin, Y.-C. Tsao, M.-Y. Yang, M. H. Huang, *Chem. Eur. J.* **2016**, *22*, 2326.
[7] D. Yu, V. W.-W. Yam, *J. Phys. Chem. B* **2005**, *109*, 5497.
[8] S. Rej, K. Chanda, C.-Y. Chiu, M. H. Huang, *Chem. Eur. J.* **2014**, *20*, 15991.
[9] K. Chanda, S. Rej, S.-Y. Liu, M. H. Huang, *ChemCatChem* **2015**, *7*, 1813.
[10] M. Kim, Y. Kim, J. W. Hong, S. Ahn, W. Y. Kim, S. W. Han, *Chem. Commun.* **2014**, *50*, 9454.
[11] C.-L. Lu, K. S. Prasad, H.-L. Wu, J.-A. A. Ho, M. H. Huang, *J. Am. Chem. Soc.* **2010**, *132*, 14546.
[12] C.-W. Yang, K. Chanda, P.-H. Lin, Y.-N. Wang, C.-W. Liao, M. H. Huang, *J. Am. Chem. Soc.* **2011**, *133*, 19993.
[13] C.-Y. Chiu, M.-Y. Yang, F.-C. Lin, J.-S. Huang, M. H. Huang, *Nanoscale* **2014**, *6*, 7656.
[14] Y.-C. Tsao, S. Rej, C.-Y. Chiu, M. H. Huang, *J. Am. Chem. Soc.* **2014**, *136*, 396.
[15] C. Chiang, M. H. Huang, *Small* **2015**, *11*, 6018.
[16] F. Wang, C. Li, L.-D. Sun, H. Wu, T. Ming, J. Wang, J. C. Yu, C.-H. Yan, *J. Am. Chem. Soc.* **2011**, *133*, 1106.
[17] S.-K. Kim, T.-J. Kim, T.-Y. Kim, G. Lee, J. T. Park, S. W. Nam, S. O. Kang, *Chem. Commun.* **2012**, *48*, 2021.
[18] P. Xi, F. Chen, G. Xie, C. Ma, H. Liu, C. Shao, J. Wang, Z. Xu, X. Xu, Z. Zeng, *Nanoscale* **2012**, *4*, 5597.
[19] D. Sun, V. Mazumder, Ö. Metin, S. Sun, *ACS Nano* **2011**, *5*, 6458.
[20] P. Verma, Y. Kuwahara, K. Mori, H. Yamashita, *J. Mater. Chem. A* **2015**, *3*, 18889.
[21] L. Hu, B. Zheng, Z. Lai, K.-W. Huang, *Int. J. Hydrogen Energy* **2014**, *39*, 20031.
[22] N.-Z. Shang, C. Feng, S.-T. Gao, C. Wang, *Int. J. Hydrogen Energy* **2016**, *41*, 944.
[23] Z. Huang, T. Autrey, *Energy Environ. Sci.* **2012**, *5*, 9257.
[24] W. Grochala, P. P. Edwards, *Chem. Rev.* **2004**, *104*, 1283.
[25] K. Fuku, R. Hayashi, S. Takakura, T. Kamegawa, K. Mori, H. Yamashita, *Angew. Chem. Int. Ed.* **2013**, *52*, 7446; *Angew. Chem.* **2013**, *125*, 7594.
[26] Q.-L. Zhu, J. Li, Q. Xu, *J. Am. Chem. Soc.* **2013**, *135*, 10210.
[27] Y.-Z. Chen, Q. Xu, S.-H. Yu, H.-L. Jiang, *Small* **2015**, *11*, 71.
[28] J. Hu, Z. Chen, M. Li, X. Zhou, H. Lu, *ACS Appl. Mater. Interfaces* **2014**, *6*, 13191.
[29] X. Huang, Y. Li, Y. Chen, H. Zhou, X. Duan, Y. Huang, *Angew. Chem. Int. Ed.* **2013**, *52*, 6063; *Angew. Chem.* **2013**, *125*, 6179.
[30] Z. Zheng, T. Tachikawa, T. Majima, *J. Am. Chem. Soc.* **2015**, *137*, 948.
[31] F. Wang, C. Li, H. Chen, R. Jiang, L.-D. Sun, Q. Li, J. Wang, J. C. Yu, C.-H. Yan, *J. Am. Chem. Soc.* **2013**, *135*, 5588.
[32] H.-L. Wu, C.-H. Kuo, M. H. Huang, *Langmuir* **2010**, *26*, 12307.
[33] P.-J. Chung, L.-M. Lyu, M. H. Huang, *Chem. Eur. J.* **2011**, *17*, 9746.
[34] N. Tian, Z.-Y. Zhou, N.-F. Yu, L.-Y. Wang, S.-G. Sun, *J. Am. Chem. Soc.* **2010**, *132*, 7580.
[35] C.-H. Kuo, L. K. Lamontagne, C. N. Brodsky, L.-Y. Chou, J. Zhuang, B. T. Sneed, M. K. Sheehan, C.-K. Tsung, *ChemSusChem* **2013**, *6*, 1993.
[36] C.-Y. Chiu, M. H. Huang, *Angew. Chem. Int. Ed.* **2013**, *52*, 12709; *Angew. Chem.* **2013**, *125*, 12941.
[37] S. Sarina, S. Bai, Y. Huang, C. Chen, J. Jia, E. Jaatinen, G. A. Ayoko, Z. Bao, H. Zhu, *Green Chem.* **2014**, *16*, 331.
[38] W.-H. Tseng, C.-Y. Chiu, S.-W. Chou, H.-C. Chen, M.-L. Tsai, Y.-C. Kuo, D.-H. Lien, Y.-C. Tsao, K.-Y. Huang, C.-T. Yeh, J.-H. He, C.-I. Wu, M. H. Huang, P.-T. Chou, *J. Phys. Chem. C* **2015**, *119*, 7554.

Received: March 28, 2016
Published online: May 3, 2016

